Available online at www.sciencedirect.com
SCIENCE DIRECT®
International Journal of Heat and Fluid Flow 25 (2004) 711–720
International Journal of HEAT AND FLUID FLOW
www.elsevier.com/locate/ijhff

Heat transfer control of a backward-facing step flow in a duct by means of miniature electromagnetic actuators

Kyoji Inaoka [a,*], Kazuya Nakamura [b], Mamoru Senda [a]

[a] Department of Mechanical and Systems Engineering, Doshisha University, Kyotanabe 610-0321, Japan
[b] Kansai Thermal Insulation Co., Ltd., Minami Senba-cho, Chuou-ku, Osaka 542-0081, Japan

Received 9 January 2004; accepted 6 May 2004
Available online 2 July 2004

Abstract

Flow and thermal control downstream of a backward-facing step has been performed in order to achieve heat transfer enhancement by introducing small disturbance with electromagnetic flap actuators on the step edge. Flap oscillation frequency and amplitude were both changed variously under the laminar flow condition. As the flap oscillation frequency increases, heat deterioration area just behind the step rapidly decreases its size until the oscillation Strouhal number Sr equals up to 0.35, but increases once and then intensively decreases again. Thus, the largest heat transfer enhancement is obtained at the highest oscillation frequency $Sr = 4.0$ within the studied frequency ranges, though sub-optimum frequency around $0.2 < Sr < 0.35$ is also obtained. From velocity measurements by PIV, it was found that intensifications of two different fluid motions, i.e., a large-scale unsteady vortex and a downward high-speed flow, are the main cause to enhance the heat transfer in the sub-optimum and in the high-frequency conditions, respectively.

Keywords: Flow separation and reattachment; Backward-facing step; Heat transfer control; Electromagnetic actuator

1. Introduction

Flow with separation and reattachment has intentionally been used for many thermo-fluidic devices as one of the heat exchange elements due to its high heat transfer performance around the flow reattachment region. In particular, as the simplest geometry to generate the flow separation and reattachment, the fundamental flow and thermal characteristics over a backward-facing step have been focused and intensively investigated both experimentally and numerically so far (Eaton and Johnston, 1981; Aung, 1983; Armaly et al., 1983; Vogel and Eaton, 1985; Kondoh et al., 1993). In terms of the heat transfer aspect, it is well known that heat transfer deterioration inevitably occurs due to the flow re-circulation just behind the step though large heat transfer enhancement is achieved downstream there. Therefore, to find the ways to recover this heat transfer deterioration is also one of the on-going research targets.

By the way, most of the available results for the backward-facing step flow in the previous studies were obtained under large aspect ratios assuming the flow and thermal fields kept two dimensional, that is, previous discussions were made about the results obtained along the centerline of the stepped channel. However, more recently, since Papadopoulos and Otugen (1995) has suggested the three dimensional flow structure of this flow system, new investigations of complex flow structures downstream the step including the effects of three dimensionality and unsteadiness have been started (Chiang and Sheu, 1999; Iwai et al., 2000; Nie and Armaly, 2002; Inaoka et al., 2002; Carrington and Pepper, 2002). Such complex flows affect thermal field and produce unique heat transfer distribution. For example, the lowest heat transfer is obtained near the side wall caused by a pair of tornado like vertical vortex and heat transfer recovery is obtained by the motion of unsteady spanwise vortex generated in the separation

* Corresponding author. Tel.: +81-774-65-6463; fax: +81-774-68-6802.
E-mail address: kinaoka@mail.doshisha.ac.jp (K. Inaoka).

0142-727X/$ - see front matter © 2004 Elsevier Inc. All rights reserved.
doi:10.1016/j.ijheatfluidflow.2004.05.006

Nomenclature

a_0	oscillation amplitude of flap actuator
f	oscillation frequency of flap actuator
Nu	local Nusselt number $= \frac{q_w S}{\lambda(T_w - T_{in})}$
Nu_s	spanwise mean Nusselt number
q_w	heat flux on the bottom wall
Re	Reynolds number $= \frac{U_m S}{\nu}$
S	step height
Sr	oscillation Strouhal number of flap actuator $= \frac{fS}{U_m}$
T_{in}	fluid temperature at the inlet
T_w	temperature on the bottom wall
U	streamwise velocity
U_m	streamwise mean velocity just upstream the step
W_D	Width of the duct
x, y, z	streamwise, wall-normal, spanwise coordinates, see Fig. 2
λ	thermal conductivity of water
ν	kinematic viscosity of water

shear layer downstream the step. Maximum heat transfer appears near the side wall region even if the flow Reynolds number is varied both for laminar and turbulent flow regime whereas the streamwise location of it moves depending on the Reynolds number (Inaoka et al., 2002).

Generally in the separation shear layer, vortex motion is well known to be quite sensitive to the initial state of the separation shear layer. This implies the possibility to control the flow and thermal characteristics by introducing the small disturbance into it. From this point of view, in order to control the flow field over the backward-facing step, various attempts by introducing different types of small periodical disturbance at the step edge have been tried both experimentally and numerically (for instance, Bhattacharjee et al., 1986; Hasan, 1992; Chun and Sung, 1996; Chun et al., 1999), and useful results have been obtained so far. Among them, a couple of common results have been observed, for example, larger disturbance achieves larger flow modification so that the flow reattachment length is drastically minimized. Another point worth to note is that an optimum disturbance frequency exists, that is, the largest flow modification or the minimum flow reattachment length is obtained at a certain disturbance frequency.

However, to the authors' knowledge, few heat transfer data are available to judge whether such flow disturbance is effective to recover the heat transfer deterioration inevitably generated behind the step. Therefore, in the present study, to see the possibility to achieve better heat transfer enhancement or heat transfer control of this flow system, a basic heat transfer experiment has been conducted when the flow has subsequently been disturbed. For this purpose, subsequent flapping of miniature electromagnetic actuator was introduced on the upstream surface of the step. Because quite unique heat transfer distributions were revealed for undisturbed duct flow with backward-facing step in the previous study (Inaoka et al., 2002), spatial distributions of heat transfer coefficient on the bottom wall downstream the step were again measured by thermo-sensitive liquid crystal sheet. In addition to that, to see the relationship between the heat transfer data and flow structure, velocity measurements by PIV were also conducted in the flow re-circulation area for the representative cases.

2. Experimental apparatus and procedures

Fig. 1 shows a schematic view of an experimental apparatus used in this study. Experiments were conducted in a close water channel consisted with an upstream tank, honeycombs, wire meshes, a contraction, a developing channel, a test section and a downstream tank. Water was driven by head difference between the upstream tank and the downstream tank. At the inlet of the test section, which was located 1500 mm downstream of the contraction, fully developed laminar flow was supplied. The test section, illustrated in Fig. 2, was 240 mm wide, 30 mm high, 500 mm long and was made of transparent acrylic plate. Since the step was 15 mm height in this study, the duct expansion ratio and the duct aspect ratio upstream the step were 2.0 and 16.0,

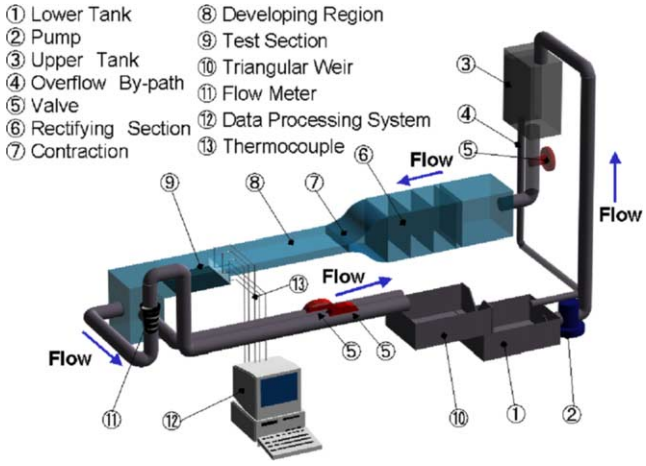

Fig. 1. Schematic view of an experimental apparatus.

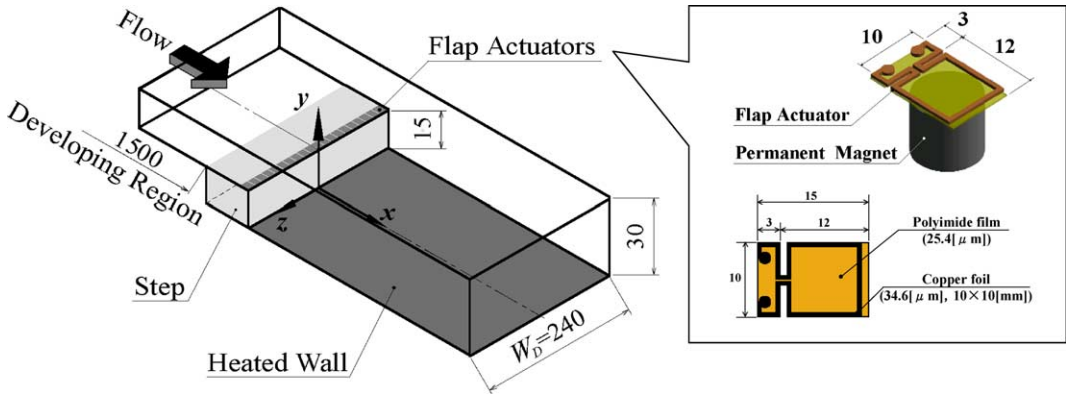

Fig. 2. Illustrations of a test section, electromagnetic flap actuator and coordinate systems.

respectively, the same value adopted in the numerical simulation by Iwai et al. (2000). The origin of the coordinate system was located at the center of the bottom line of the backward-facing wall. *x*-, *y*- and *z*-coordinates were set for the streamwise, the wall-normal and the spanwise directions, respectively.

In the heat transfer experiment, distributions of the local heat transfer coefficient on the bottom wall downstream of the step were measured by making use of a thermo-sensitive liquid crystal sheet. For this, as shown in Fig. 3, inner surface of the bottom plate was covered with thin stainless steel foil strips of 39.5 mm wide, 500 mm long and 20 μm thick, having 1 mm spanwise spacing with each other. These foil strips were connected electrically in series and were heated by passing an alternating current through them, that is, a constant heat flux heating condition was established at the wall. Though the side walls were not heated in this study, an additional heating of side walls made only small difference in the heat transfer distribution on the bottom wall in the preliminary study. The liquid crystal sheet of 75 μm thick was glued between the heater strips and the transparent bottom wall so as to monitor the local distributions of the bottom wall temperature. Color images of the liquid crystal sheet were subsequently taken with a CCD video camera through the transparent bottom plate from outside of the test section and were converted to the temperature distributions by making use of a supervised learning of hierarchy neural network system (Kimura et al., 1993). In the present heat transfer experiment, totally more than 32 images taken at appropriate intervals were used to obtain the time-averaged distribution. The calibration of the image conversion was done prior to every heat transfer measurement. To evaluate the local heat transfer characteristics in the following discussion, the local Nusselt number defined based on the step height *S* as Eq. (1) will be used.

$$Nu = \frac{q_w S}{\lambda(T_w - T_{in})}, \tag{1}$$

where λ is the thermal conductivity of the fluid, T_w is the local wall temperature and T_{in} is the inlet fluid temperature. The constant wall heat flux q_w was calculated from the electric power input through the stainless foil strips. Heat conduction loss toward the outside of the duct was neglected since its value was less than 0.3% of the total heat flux. Uncertainty of the bottom wall temperature using the liquid crystal sheet was less than 0.18 K in the present study (Inaoka et al., 2002). This produced the largest uncertainty of the local Nusselt number less than 4% at the maximum heat transfer location where the smallest temperature difference between the wall and fluid temperatures was generated.

To give small disturbance to the initial state of the separation shear layer, electromagnetic actuators made of polyimide thin film (Suzuki et al., 1999) were introduced at the step edge. Totally 20 sets of a miniature thin actuator (10 mm wide, 15 mm long and 25 μm thick each) and a permanent magnet (10 mm diameter, 10 mm long and 4900 G magnetic flux each) were placed spanwisely on the upstream surface of the step. Each

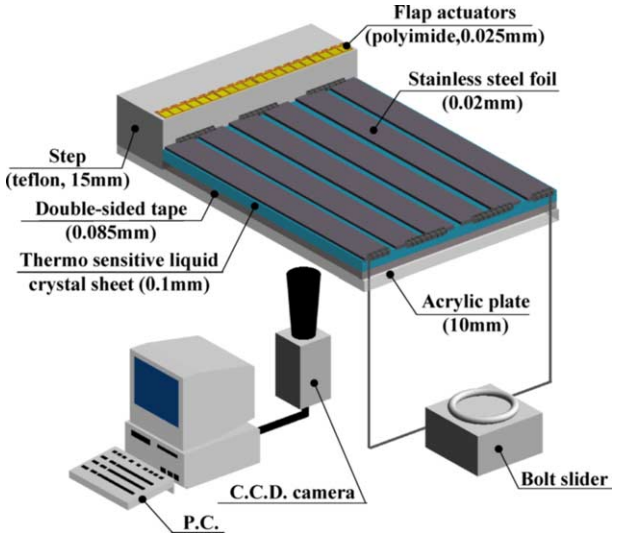

Fig. 3. Schematic view of a test plate for the heat transfer experiment.

flap actuator was set as its trailing edge was coincided with the step edge and the permanent magnet was correspondingly embedded so as that its top surface was flush with the upstream surface of the step. Since each spanwise space between the neighbor actuators was 2 mm, the ratio of spanwise width where the actuators were arranged to the duct whole width was about 0.83. By passing a current through the copper circuit (35 μm thick) made on the polyimide film, a magnetic field was established around the circuit. Due to the interaction between this magnetic field and the permanent magnet, this electromagnetic actuator can elastically change its position to plus and minus y directions except for its upstream part (2 mm length) given as a fulcrum. By passing a programmed current through the circuit, an appropriate time-dependent oscillatory actuation, open and close motions, can be achieved for each discrete flap actuator. Flap oscillation frequency f and amplitude a_0, i.e., time-dependent displacement between the trailing edge of the flap and the step wall was monitored during the experiment by laser displacement meter. Its typical behavior was shown for example in Fig. 4. As a basic experiment in the present study, the simplest disturbance condition was adopted, that is, every actuator oscillates at the same time by introducing the same driving signal to every actuator. As experimental parameters, flap oscillation frequency f and amplitude a_0 were both changed variously under the laminar flow condition, $Re = 1000$ as for the first try. Here, Reynolds number is defined based on step height S and streamwise mean velocity U_m as Eq. (2).

$$Re = \frac{U_m S}{\nu}, \tag{2}$$

where ν is the kinematic viscosity of water. Because the largest heat transfer deterioration area has been obtained at $Re = 1000$ among other Reynolds number cases including turbulent flow regime in the previous study (Inaoka et al., 2002), the present Reynolds number case is expected to generate the largest effect to minimize the heat transfer deterioration if the flap oscillation works effectively. In the present Reynolds number of 1000, just upstream the step, the streamwise

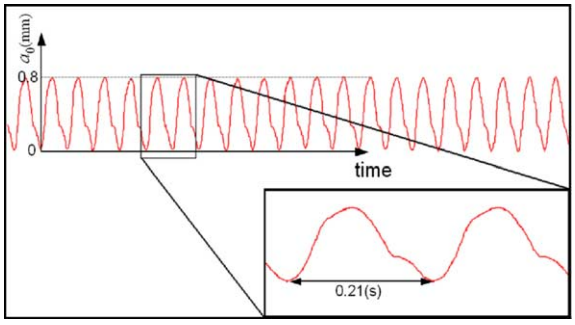

Fig. 4. Example of the time-dependent displacement of the actuator ($a_0 = 0.8$ mm, $f = 4.7$ Hz ($Sr = 1.0$)).

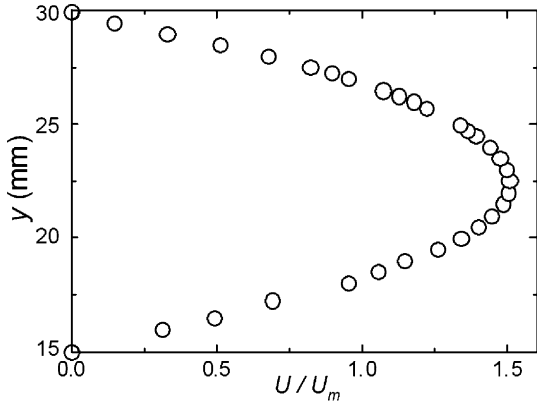

Fig. 5. Wall-normal distribution of the streamwise velocity at the center of the duct just upstream the step.

velocity shows a parabolic shape at the center of the duct like in Fig. 5. Two conditions were examined. At first as for a case A, to see the effect of oscillation frequency, keeping the flap oscillation amplitude $a_0 = 0.8$ mm, the flap oscillation frequency was changed in 33 steps ranging from 0 (without actuation) to 18.8 Hz. This corresponds to the change of the flap oscillation Strouhal number Sr, defined based on the step height and mean velocity as Eq. (3), from 0.0 to 4.0.

$$Sr = \frac{fS}{U_m}. \tag{3}$$

Next as for a case B, to see the effect of oscillation amplitude, oscillation amplitude a_0 was changed in 18 steps ranging from 0 to 2.4 mm under two representative flap oscillation frequencies $Sr = 0.2$ and 1.0.

To grasp the flow structure downstream the step, flow visualization was also carried out. For the representative cases, especially in the case A, instantaneous velocity vectors in x–y plane along the centerline of the duct and those in x–z plane near the bottom wall were measured by 2D-PIV system. For this, nylon powders of 50 μm diameter and 30 mJ Nd:YAG double pulse laser source were used. The measurement areas in x–y and x–z planes are respectively 75×30 mm^2 ($5S \times 2S$) and 100×90 mm^2 ($6.7S \times 6S$). The thickness of the laser sheet was about 1.0 mm for both cases. The particle images were acquired by a cross-correlation camera (1018×1008 pixel^2) at 30 frames/s and recorded onto a hard disc of a personal computer. Velocity vectors were calculated using cross-correlation method combined with post median filtering for removing spurious vectors.

3. Results and discussion

3.1. Distributions of heat transfer coefficient on the bottom wall

Fig. 6 shows the distributions of the local Nusselt number Nu in the representative cases of A, constant

amplitude ($a_0 = 0.8$ mm) condition, (a) without actuation and with flap oscillation (b) $Sr = 0.2$, (c) $Sr = 1.0$ and (d) $Sr = 4.0$, respectively. Indexed color scales drawn in the figure correspond to the value of the local Nusselt number. Dark gray parts correspond to the area of high Nusselt number whereas light-colored parts to that of low Nusselt number. First of all, unique distributions of the local Nusselt number without actuation case (Fig. 6(a)) should shortly be reviewed. Relatively large high Nusselt number area, observed around $5 < x/S < 15$, shows heat transfer enhancement basically produced by the flow reattachment. Upstream that and just behind the step, there exists large area of low Nusselt number or heat transfer deterioration which we want to recover in the present study. Other unique points worth to mention are the maximum heat transfer appears in two regions near the side walls and the lowest heat transfer appears also in two regions near the side walls just behind the step.

Noticeable effects of the flap oscillation can be found in Fig. 6(b)–(d). For every case with flap oscillation, heat deterioration area just behind the step remarkably reduces its size compared to that without actuation. Thus, heat transfer recovery is found to obtain by this flap actuation. According to this size change, the maximum peak of the heat transfer coefficient changes its position streamwisely closer to the step. This tendency is something similar to that observed in the effect of increasing Reynolds number from 1000 to 2300 in the previous study (Inaoka et al., 2002). On the contrary, seen in Fig. 7, spanwise position of the maximum heat transfer appears almost near the side wall region. In this sense, side wall effect still remains large for the disturbed case in this type of flow system.

To see this point more in detail, Fig. 8 shows the streamwise locations of the downstream edge of heat transfer deterioration area for various Sr cases. Here, heat transfer deterioration area just behind the step was chosen where the spanwise mean Nusselt number showed lower value than the spatial mean value for the whole test section. As the oscillation frequency increases, heat transfer deterioration area rapidly decreases its size until around $0.2 < Sr < 0.35$. However, it increases up to around $Sr = 1.0$ and then it gradually decreases again. Within the studied conditions, minimum streamwise position was obtained at the highest frequency $Sr = 4.0$ in the present study. Thus, suboptimum value of heat transfer recovery was obtained around $0.2 < Sr < 0.35$, and the largest heat transfer recovery was achieved at $Sr = 4.0$. The former decreasing tendency of heat transfer deterioration with increasing frequency is very interesting because similar

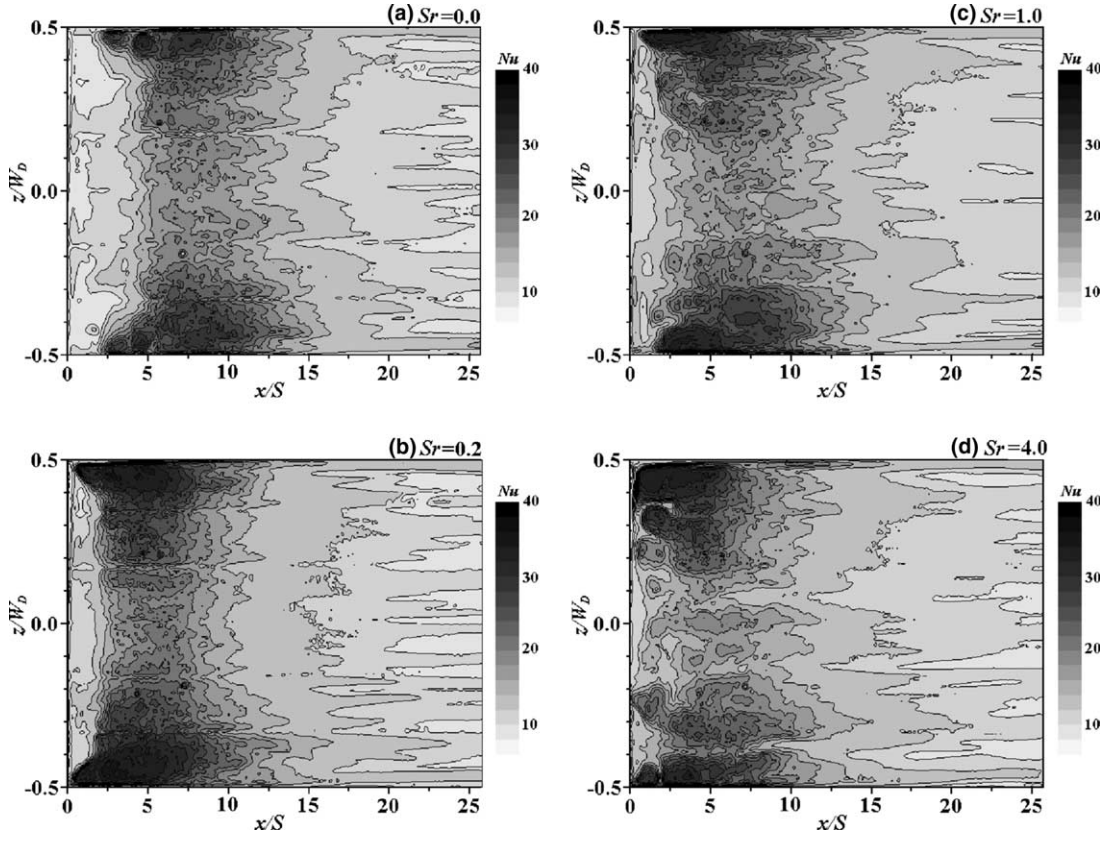

Fig. 6. Distributions of the local Nusselt number on the bottom wall for the representative Sr cases (case A, $a_0 = 0.8$ mm).

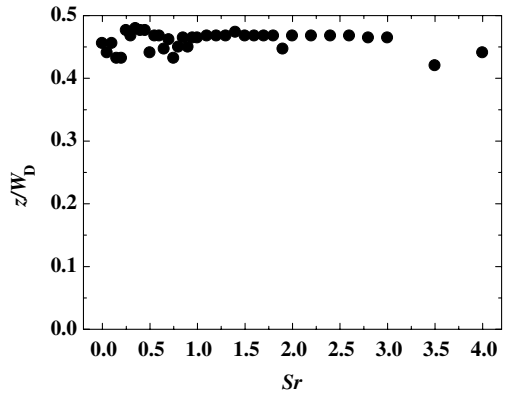

Fig. 7. Spanwise locations of the maximum Nusselt number for various Sr cases (case A, $a_0 = 0.8$ mm).

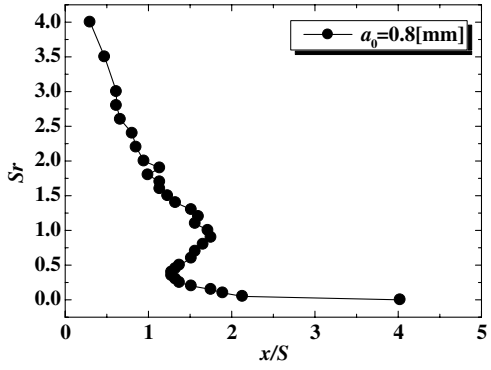

Fig. 8. Streamwise locations of the downstream edge of the low Nusselt number area (case A, $a_0 = 0.8$ mm).

optimum frequencies for the minimum flow reattachment length have been achieved by other research groups though they were in the turbulent flow regime. For example, the results by Chun et al. (1999), where the periodical flow disturbance was given by blowing and suction, the flow reattachment length became minimum at the similar optimum value of $Sr = 0.27$. However, the latter decreasing tendency of high Sr case has never been reported in the previous literatures. Although further investigation would be needed because such latter decreasing tendency of heat transfer recovery was never found in the results from the reattachment point of view, however, the present heat transfer results show some possibility to generate shorter reattachment length, especially in laminar flow regime by providing higher frequent disturbance at the step edge.

Fig. 9 shows the streamwise distributions of the spanwise mean Nusselt number, Nu_s for the corresponding cases in Fig. 6. Heat transfer recovery just behind the step and the upstream shift of the heat transfer enhancement can be reconfirmed for disturbed cases. Interestingly, the maximum value of Nu_s in the sub-optimum frequency of $Sr = 0.2$ becomes larger than that without actuation case while those in other two cases of $Sr = 1.0$ and 4.0 show almost the same as that without actuation. In this case of sub-optimum frequency, intensive heat transfer enhancement is achieved though the recovery area is relatively smaller than other frequency cases. This suggests the difference in the flow structure and it will be mentioned later.

On the other hand, in case B of the constant frequency condition, strong effect of the oscillation amplitude a_0 on the heat transfer recovery was also worth to mention. Fig. 10 shows how oscillation amplitude a_0 augments the heat transfer recovery for two representative frequency cases. It was clearly found that even small amplitude can effectively reduce the heat transfer deterioration for both oscillation frequency cases. The larger oscillation amplitude becomes, the more effective heat transfer recovery is generated, although its effectiveness becomes almost constant at large amplitude oscillation. Fig. 11 shows the streamwise distributions of spanwise mean Nusselt number for the representative amplitude cases of $Sr = 0.2$. From this

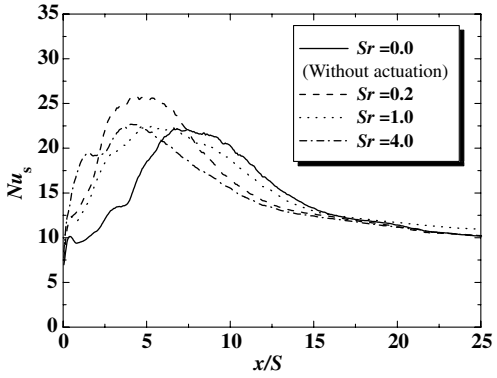

Fig. 9. Streamwise distributions of the spanwise mean Nusselt number, Nu_s (case A, $a_0 = 0.8$ mm).

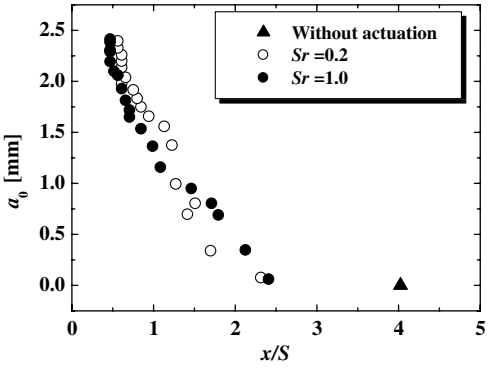

Fig. 10. Streamwise locations of the downstream edge of the low Nusselt number area (case B, $Sr = 0.2$ and 1.0).

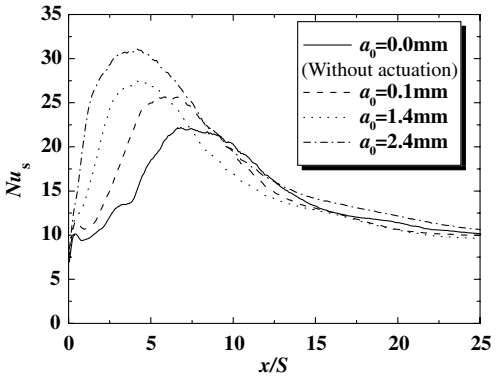

Fig. 11. Streamwise distributions of spanwise mean Nusselt number, Nu_s (case B, $Sr = 0.2$).

figure, intensive large heat transfer enhancement is confirmed downstream the step and this contributes to reduce the heat transfer deterioration area for large amplitude case. The large amplitude achieves the large heat transfer enhancement.

3.2. Flow structure related to the heat transfer enhancement

Fig. 12 shows the magnified view of the local Nusselt number and corresponding time-averaged velocity vectors near the bottom wall obtained by PIV for the three representative cases, (a) without actuation, (b) $Sr = 0.2$ and (c) $Sr = 4.0$, respectively. Basically, in the case without actuation, low Nusselt number area corresponds well to the low-speed flow area behind the step. Thus, such low-speed flow is the main cause of the heat transfer deterioration. Especially near the side wall, weak but clockwise fluid motion can be found. Although further 3-D PIV measurements would be needed to quantitatively examine this fluid motion, this is what is called tornado like vertical vortex (Papadopoulos and Otugen, 1995) and we can find from this figure that this vortex results in generating the lowest Nusselt number there. On the other hand, the location of relatively high-speed flow corresponds well to the high Nusselt number area. Such high-speed flow, though it is reversed flow, is basically brought by the downward flow from the main stream and it enhances the heat transfer there. In the case of $Sr = 0.2$, much more complicated flow structure can be observed. Owing to this flow change, low-speed flow area becomes so small so that the low Nusselt number area intensively reduces its size. In the case of $Sr = 4.0$, it is very difficult to find low-speed flow or even reverse flows. Thus, flow structure is completely changed from what we observed for undisturbed case.

Fig. 13 shows typical snapshots of the instantaneous velocity vector along the centerline of the stepped duct

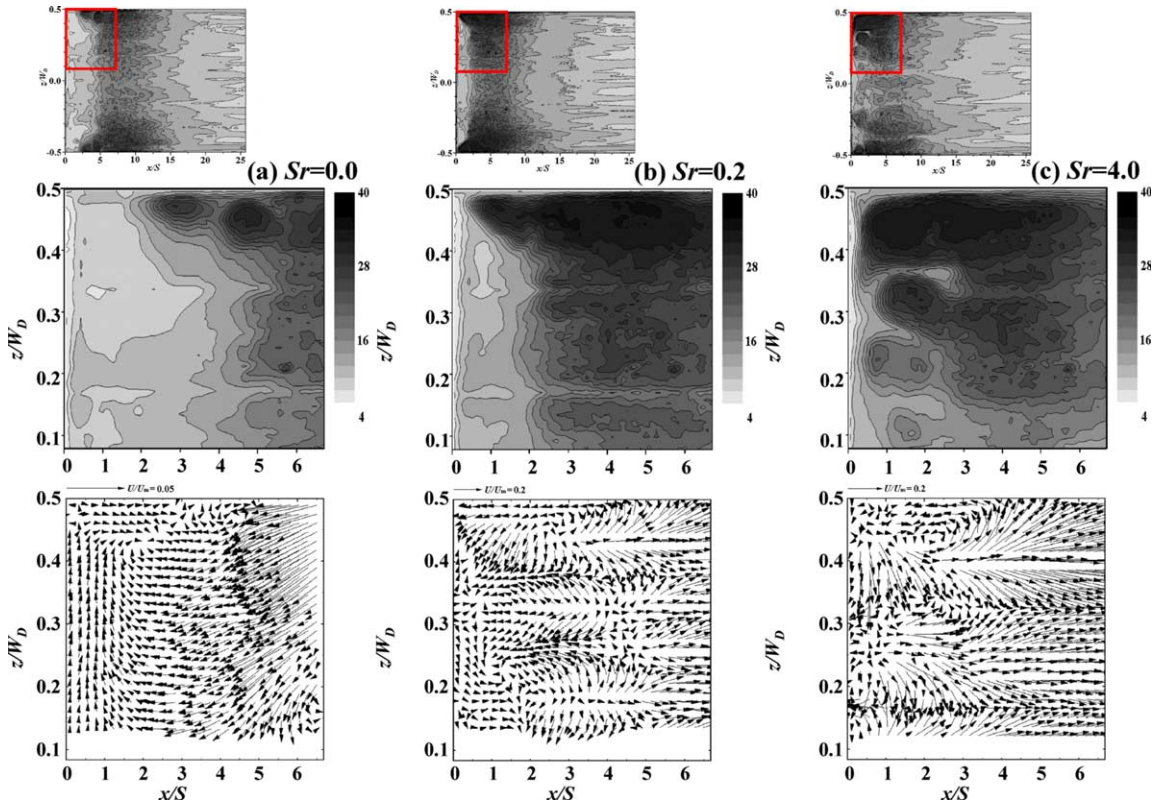

Fig. 12. Magnified view of the local Nusselt number and time-averaged velocity vectors near the bottom wall for case A.

measured by PIV for representative frequency conditions in case A, (a) without actuation $Sr = 0.0$, (b) sub-optimum frequency at $Sr = 0.2$, (c) high frequency at $Sr = 4.0$. Here, streamwise distribution of the local Nusselt number on the bottom wall along the centerline of the duct was correspondingly shown below in the figure. In the basic case without actuation, stable separated shear layer is observed toward downstream from the step edge. The flow inside the re-circulation area has very low reverse velocity component and the downstream regions of $0 < x < 4S$ confirms almost stagnant at this low Reynolds number $Re = 1000$. Because the area of heat transfer deterioration corresponds well to that of the stable flow stagnation, this stable flow stagnation is the main cause of the heat transfer deterioration behind the step.

In the case of $Sr = 0.2$, just downstream the step edge, small upward fluid motion from the re-circulation area toward the top wall was observed. This upward fluid motion is synchronizingly generated when the trailing edge of the actuator flaps up to the wall normal direction. Fig. 14 shows the time series of the obtained unsteady flow structures. From this figure, we can find that the small upward fluid motion develops entraining faster fluid from the main stream, pushing the slow stagnant fluid to the main stream and changing its elevation to the bottom wall, thus, unsteady vortex is subsequently generated as it goes downstream in the separated shear layer. This unsteady vortex develops larger as it goes downstream and becomes wide almost comparable to the step size. This unsteady vortex finally joins to the main flow and it impinges the main flow toward the bottom wall. This intensive vortex development and above flow impingement contribute largely to minimize the flow reattachment length. This large-scale unsteady vortex basically supplies cold fresh fluid of the main stream to the bottom wall and pushes the hot fluid near the wall toward main stream, it acts washing the hot bottom wall or mixing the fluid in the re-circulation area. As can be seen in Fig. 13(b), the area where this vortex comes near the bottom wall corresponds well to

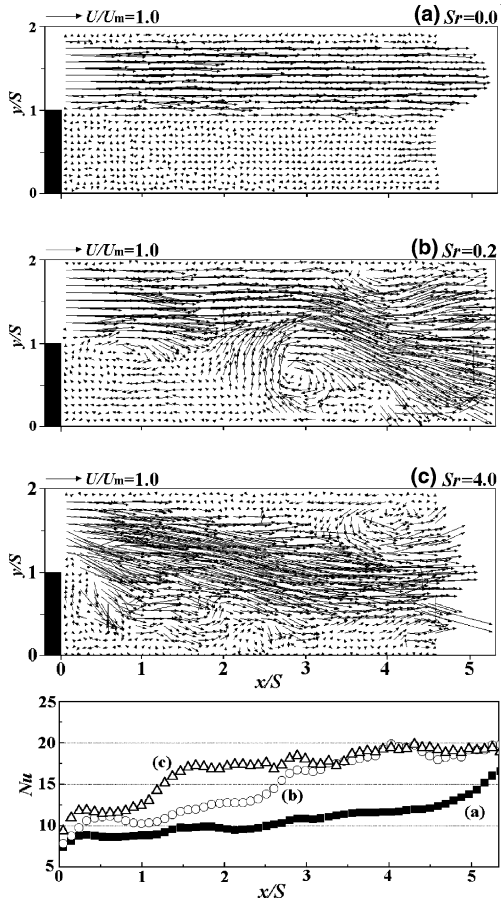

Fig. 13. Instantaneous velocity vectors and the local Nusselt number along the duct centerline (case A, $a_0 = 0.8$ mm).

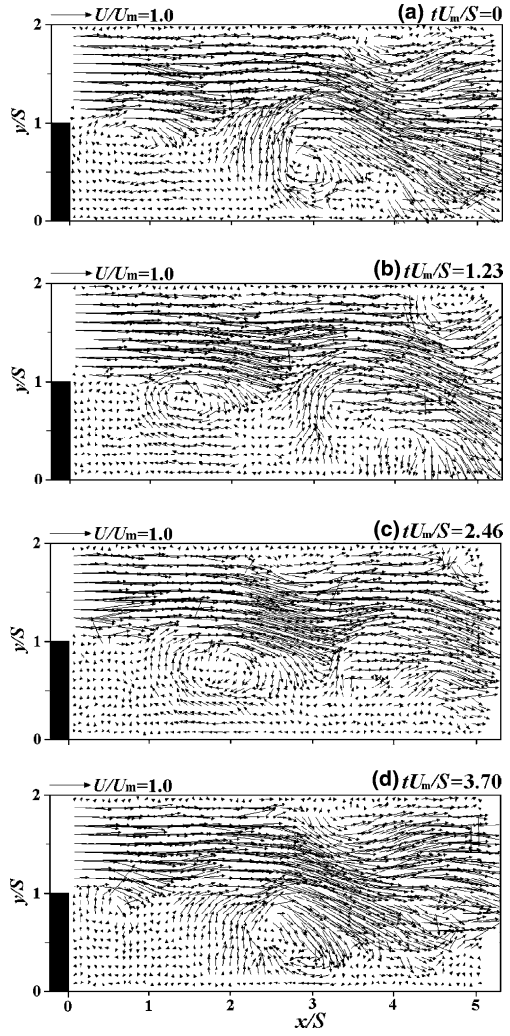

Fig. 14. Vortex behavior with time for sub-optimum oscillation case at $Sr = 0.2$.

that of heat transfer recovery, therefore, the main cause of the sub-optimum frequency is the periodical generation of this large-scale unsteady vortex.

In the case of $Sr = 4.0$, as can be seen in Fig. 13(c), a completely different flow structure was observed from that seen in Fig. 13(b). In this time, no large-scale vortex motion but an intensive downward fluid motion of a portion of high-speed main stream can be observed just behind the step. This high-speed downward flow then sweeps near the bottom wall producing irregular velocity fluctuations behind the step, and as a result, it plays a role to break the stable flow re-circulation so that flows downstream of the step are no longer stagnant. Interestingly, the whole direction of the main stream was also distorted toward the bottom wall. The area of heat transfer recovery agrees well to the area where velocity fluctuations are observed near the bottom wall. Therefore, the main cause of the maximum heat transfer enhancement in the optimum high-frequency case within the studied frequency ranges is this intensive high-speed downward flow, which is different from that of the sub-optimum case. In the intermediate frequency case, especially around $Sr = 1.0$, it is expected that the flow transition occurs from the flow field characterized by the large-scale unsteady vortex to that characterized by the high-speed downward flow. Because of the trade-off relation between these two flow structures, either cause of heat transfer enhancement is weakened around $Sr = 1.0$.

4. Concluding remarks

Heat transfer experiment has been done on a duct flow with a backward-facing step where a small disturbance has been introduced by flap actuators to achieve heat transfer recovery behind the step. Spatial distributions of local heat transfer coefficients on the bottom wall were measured for various flap oscillation frequencies and amplitudes under laminar flow conditions. Velocity measurements by PIV have also been conducted to see the flow structures related to the heat transfer recovery. Main results obtained in this study are summarized as follows.

A flap oscillation was very effective to recover the heat transfer deterioration or to enhance the heat transfer behind the step. As the oscillation frequency increases, heat transfer deterioration area behind the step rapidly decreases its size until the oscillation Strouhal number around $0.2 < Sr < 0.35$, but increases once and then intensively decreases again. Thus, an oscillation with the highest frequency at $Sr = 4.0$ achieves the best heat transfer recovery within the experimental frequency ranges, though oscillation with sub-optimum frequency around $0.2 < Sr < 0.35$ is also obtained from the heat transfer point of view. Two different types of fluid motions, an unsteady large-scale vortex periodically produced in the separation shear layer and a high-speed downward flow from the main stream, are the main cause of the heat transfer recoveries for different oscillation frequencies, $0.2 < Sr < 0.35$ and $Sr = 4.0$, respectively. Flap oscillation with small amplitude is still effective to reduce heat transfer deterioration. The larger the oscillation amplitude is, the larger heat transfer enhancement is obtained within the studied amplitude ranges.

Acknowledgements

This work was supported through the research project on "Micro Gas Turbine/Fuel Cell Hybrid-type Distributed Energy System" by the Department of Core Research for Evolutional Science and Technology (CREST) of the Japan Science and Technology Corporation (JST).

References

Aung, W., 1983. An experimental study on laminar heat transfer downstream of backsteps. J. Heat Transfer 105, 823–829.

Armaly, B.F., Durst, F., Pereira, J.C.F., Schonung, B., 1983. Experimental and theoretical investigation of backward-facing step flow. J. Fluid Mech. 127, 473–496.

Bhattacharjee, S., Scheelke, B., Troutt, T.R., 1986. Modification of Vortex Interactions in a Reattaching Separated Flow. AIAA J. 24 (4), 623–629.

Carrington, D.B., Pepper, D.W., 2002. Convective heat transfer downstream of a 3-D backward-facing step. Numer. Heat Transfer Part A 41, 555–578.

Chiang, T.P., Sheu, T.W.H., 1999. A numerical revisit of backward-facing step flow problem. Phys. Fluid 11, 862–874.

Chun, K.B., Sung, H.J., 1996. Control of turbulent separated flow over a backward-facing step by local forcing. Exp. Fluids 21, 417–426.

Chun, S., Lee, I., Sung, H.J., 1999. Effect of spanwise-varying local forcing on turbulent separated flow over a backward-facing step. Exp. Fluids 26, 437–440.

Eaton, J.K., Johnston, J.P., 1981. A review of research on subsonic turbulent flow reattachment. AIAA J. 19 (9), 1093–1100.

Hasan, M.A.Z., 1992. The flow over a backward-facing step under controlled perturbation—laminar separation. J. Fluid Mech. 238, 73–96.

Inaoka, K., Kojima, T., Nakamura, K., Senda, M., 2002. Heat transfer characteristics of 3-D backward-facing step flow in a rectangular duct. Proc. 13th Int. Symp. on Transport Phenomena, 267–272.

Iwai, H., Nakabe, K., Suzuki, K., 2000. Flow and heat transfer characteristics of backward-facing step laminar flow in a rectangular duct. Int. J. Heat Mass Transfer 43 (3), 457–471.

Kimura, I., Kuroe, Y., Ozawa, M., 1993. Application of neural networks to quantitative flow visualization. J. Flow Visualization Image Process. 1, 261–269.

Kondoh, T., Nagano, Y., Tsuji, T., 1993. Computational study of laminar heat transfer downstream of a backward-facing step. Int. J. Heat Mass Transfer 36, 577–591.

Nie, J.H., Armaly, B.F., 2002. Three-dimensional convective flow adjacent to backward-facing step—effects of step height. Int. J. Heat Mass Transfer 45, 2431–2438.

Papadopoulos, G., Otugen, M.V., 1995. Separating and reattaching flow structure in a suddenly expanding rectangular duct. J. Fluids Eng. 117, 17–23.

Suzuki, H., Kasagi, N., Suzuki, Y., 1999. Active control of an axisymmetric jet with an intelligent nozzle. Proc. 1st Int. Symp. on Turbulence and Shear Flow Phenomena, 665–670.

Vogel, J.C., Eaton, J.K., 1985. Combined heat transfer and fluid dynamic measurements downstream of a backward-facing step. Trans. ASME 107, 922–929.